The Journal of Chemical Physics

RESEARCH ARTICLE | MAY 17 2023

Dynamics of the Cl^- + CH_3I reaction on a high-level *ab initio* analytical potential energy surface

András B. Nacsa ; Viktor Tajti ; Gábor Czakó

J. Chem. Phys. 158, 194306 (2023)
https://doi.org/10.1063/5.0151259

AIP Publishing

The Journal of Chemical Physics ARTICLE scitation.org/journal/jcp

Dynamics of the $Cl^- + CH_3I$ reaction on a high-level *ab initio* analytical potential energy surface

Cite as: J. Chem. Phys. 158, 194306 (2023); doi: 10.1063/5.0151259
Submitted: 20 March 2023 • Accepted: 30 April 2023 •
Published Online: 17 May 2023

András B. Nacsa, Viktor Tajti, and Gábor Czakó[a]

AFFILIATIONS

MTA-SZTE Lendület Computational Reaction Dynamics Research Group, Interdisciplinary Excellence Centre and Department of Physical Chemistry and Materials Science, Institute of Chemistry, University of Szeged, Rerrich Béla tér 1, Szeged H-6720, Hungary

[a]Author to whom correspondence should be addressed: gczako@chem.u-szeged.hu

ABSTRACT

We have developed a full-dimensional analytical *ab initio* potential energy surface (PES) for the $Cl^- + CH_3I$ reaction using the ROBOSURFER program system. The energy points have been computed using a robust composite method defined as CCSD-F12b + BCCD(T) – BCCD with the aug-cc-pVTZ(-PP) basis set and have been fitted by the permutationally invariant polynomial approach. Quasi-classical trajectory simulations on the new PES reveal that two product channels are open in the collision energy (E_{coll}) range of 1–80 kcal/mol, i.e., S_N2 leading to $I^- + CH_3Cl$ and iodine abstraction (above ~45 kcal/mol) resulting in $ICl^- + CH_3$. Scattering angle, initial attack angle, product translational energy, and product internal energy distributions show that the S_N2 reaction is indirect at low E_{coll} and becomes direct-rebound–back-side (CH_3-side) attack-type, as E_{coll} increases. Iodine abstraction mainly proceeds with direct stripping mechanism with side-on/back-side attack preference. Comparison with crossed-beam experiments and previous direct dynamics simulations shows quantitative or qualitative agreement and also highlights possible theoretical and/or experimental issues motivating further research.

I. INTRODUCTION

The reaction of the chloride ion (Cl^-) with methyl-iodide (CH_3I) is one of the prototypes of bimolecular nucleophilic substitution (S_N2), therefore attracting considerable attention both by theory and experiment.[1–9] In 2008, the $Cl^- + CH_3I$ reaction played a key role in testing the novel crossed-beam setup of Wester and co-workers[2] and challenged the Hase group[2,4] to perform realistic direct dynamics simulations. The joint experimental–theoretical effort provided unprecedented insights into the atomic-level dynamics of an S_N2 reaction revealing a new roundabout pathway and showing that these reactions are much more complex than the traditional back-side attack Walden-inversion picture suggests.[2] Following the electronic structure study of Hase and co-workers,[3] which only considered the pre- and post-reaction ion–dipole complexes and the Walden-inversion transition state, and building on the results obtained for other S_N2 reactions,[10–15] in 2017[5] we reported a comprehensive benchmark coupled-cluster-based *ab initio* characterization of the title reaction revealing several novel stationary points, such as hydrogen- and halogen-bonded complexes,[9–13,16] front-side attack and double-inversion[14,15] transition states, as well as many minima and saddle points along the proton-transfer channel. Dynamics simulations for the $Cl^- + CH_3I$ reaction are so far restricted to the use of the direct dynamics approach,[2,4,8] which computes the electronic energies and gradients on-the-fly making the trajectory evaluation very time-consuming even if a low level of electronic structure theory is applied.

In the present study, we plan to report the first analytical full-dimensional potential energy surface (PES) for the title reaction, which allows using high-level of *ab initio* theory and efficiently computing a large number of trajectories, thereby ensuring high accuracy from both electronic structure and statistical aspects. The PES development utilizes the ROBOSURFER program package,[17] which automatically selects new configurations along trajectories, performs *ab initio* computations, adds energy points to the dataset, and fits the energies using the permutationally invariant polynomial approach,[18,19] thereby iteratively improving the PES. On the new PES, we perform quasi-classical trajectory (QCT) computations for the $Cl^- + CH_3I$ reaction allowing direct comparison to crossed-beam experiments[2,4,7] and previous direct dynamics simulations.[2,4] Existing disagreements between experimental and direct dynamics results may come from the limitations of the electronic structure

method and basis set as well as from the classical nature of the QCT method. The new high-level coupled-cluster-based PES may help to clarify the effect of the electronic structure theory on the dynamics results. Furthermore, experiments provide detailed differential cross section data, such as scattering angle and product internal energy distributions, whose precise simulations were very challenging for direct dynamics because of their low statistical accuracy. The analytical PES enables the computations of orders of magnitude more trajectories compared to on-the-fly dynamics, thereby providing statistically accurate differential cross sections like crossed-beam experiments. The computational details of the PES development are described in Sec. II. The results are presented, discussed, and compared with previous experimental and theoretical data in Sec. III. The paper ends with a summary and conclusions in Sec. IV.

II. COMPUTATIONAL DETAILS

We generate an initial dataset of geometries based on the stationary points[5] of the reactive PES: we randomly displace the Cartesian coordinates of atoms of these points in the 0.0–0.4 Å regime, and in the case of the reactants and products, we scatter the displaced molecules/ions randomly around each other in the range of 2.0–10.0 Å. We perform single-point computations with the aug-cc-pVTZ(-PP) basis set,[20,21] applying a relativistic effective core potential for iodine,[21] using a composite CCSD(T)-F12b method,[22] where the parenthesis T contribution is calculated from the BCCD(T) energies,[23] thereby avoiding any serious unphysical breakdown of the perturbative (T) correction at strongly correlated regions (see Ref. 24 for details). All the *ab initio* computations are carried out utilizing the MOLPRO program package.[25] Structures with higher relative energy (to the global minimum of this set) than 100 kcal/mol are excluded from our starting batch. After this, we fit a primitive PES with the permutationally invariant-polynomial method.[18,19] Further development is performed by the ROBOSURFER program system[17] iteratively. ROBOSURFER adds new geometries to the set based on QCT results at nine different collision energies: 1, 10, 20, 30, 40, 50, 60, 70, and 80 kcal/mol, respectively. The highest total polynomial order used in the fitting function is fifth and the fitting itself is done by using a least-squares fit with weights of $E_0/(E + E_0)$, where E is the potential energy relative to the minimum of the fitting set and E_0 = 0.1 hartree. To improve accuracy in the higher energy regions, we manually added points for the $H^- + CH_2ClI$ and the $CH_2 + I^- + HCl$ low-probability reaction channels to achieve the desired accuracy for them. Finally, we have 3313 coefficients based on 9048 points, with 0.61, 1.29, and 1.75 kcal/mol root-mean-square fitting errors in the 0–62.75, 62.75–125.5, and 125.5– kcal/mol intervals, relative to the global minimum, respectively.

To investigate the dynamics of the $Cl^- + CH_3I$ reaction, we analyze QCTs at 11 different collision energies (E_{coll}): 1, 3.75, 8.99, 10.38, 17.53, 24.67, 43.81, 50.00, 60.00, 70.00, and 80.00 kcal/mol. These trajectories are computed on the previously developed analytical PES. At the beginning of each trajectory, we set the system to the quasi-classical ground vibrational state by the standard normal-mode sampling[26] [giving the reactant zero-point energy (ZPE)]. The reactants were randomly oriented in the space, and the starting distance between them is $\sqrt{x^2 + b^2}$, where x is 25 bohrs (except at 1 kcal/mol E_{coll}, where x is 40 bohrs), while we vary the b impact parameter from 0.0 to b_{max} with a 0.5 bohrs step size. One reaches b_{max} when there are no reactive collisions, in our case the highest one is 26.5 bohrs (at 1 kcal/mol E_{coll}). At every b and E_{coll}, we evaluate 5000 trajectories, in total, which means more than 1.5×10^6 trajectories. These are propagated with a 0.0726 fs time step until a geometrical criterion is reached: the largest interatomic distance becomes greater than the original largest by 1 bohr. We calculate reaction probabilities, and for substitution reactions, we distinguish retention and inversion with a vector projection scheme.[27] The excitation functions [integral cross sections (ICSs) as a function of E_{coll}] are resolved with soft and hard ZPE restrictions. The former means that we exclude trajectories where the total vibrational energy of the products is less than the sum of their ZPEs. In the latter case, we exclude trajectories when either one of the products has less vibrational energy than its ZPE. For every reaction channel, we also take account of the scattering and the initial attack angle (for definition, see Fig. 1) distributions, the products' relative translational energy distribution, the internal energy distribution of every product, and their rotational quantum numbers.

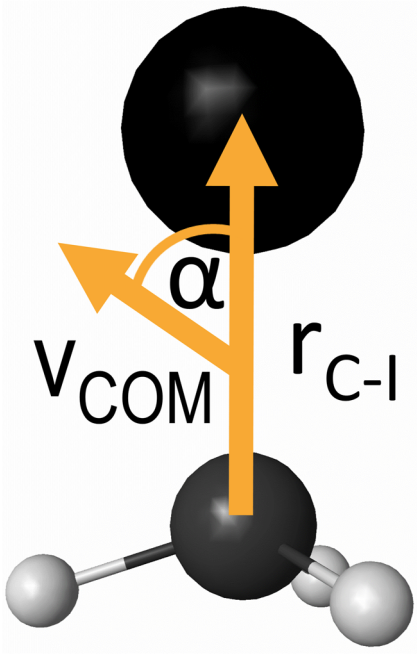

FIG. 1. The definition of the initial attack angle: the angle between the vector of the C–I bond and the center of mass velocity vector.

III. RESULTS AND DISCUSSION

A. The PES

The schematic energy diagram of the $Cl^- + CH_3I$ reaction is shown in Fig. 2. For the different reaction channels, we indicate the benchmark[5] classical relative energies of the different transition states and minima with the energies obtained on our PES. The only exothermic reaction is the S_N2, with the reaction heat of −14.47 kcal/mol. This channel is barrierless since all of the transition

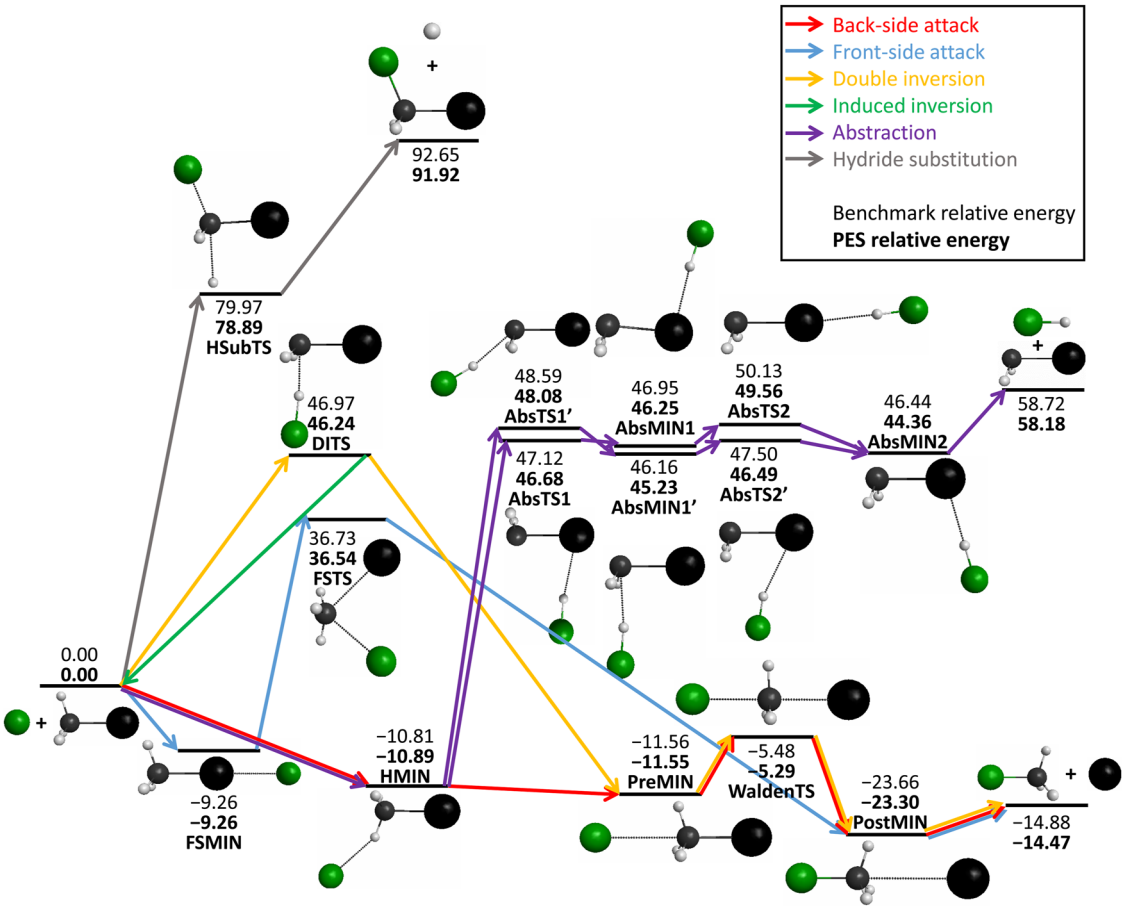

FIG. 2. The schematic energy diagram of the $Cl^- + CH_3I$ reaction, comparing the classical relative energies obtained on the present analytical PES with all-electron CCSDT(Q)/complete-basis-set-quality benchmark results (Ref. 5). The energies are given in kcal/mol.

states and minima are under the energy level of the reactants. This reaction can also happen via retention (front-side attack and double-inversion mechanisms), but this way barriers emerge, as the formation of the initial transition states are endothermic. The proton-abstraction is highly endothermic, 58.18 kcal/mol, while the related minima and transition states are under the energy level of the products. It can also be seen that the S_N2 reaction's barriers are lower, even with the double-inversion path, than the formation of HCl. Another possible reaction is the very endothermic hydride substitution (91.92 kcal/mol). Proton-abstraction or hydride-substitution reactions do not take place with the conditions of our simulations, we mainly observe the S_N2 reaction (back-side attack) and at higher energies iodine abstraction leading to $CH_3 + ICl^-$, which has a reaction heat of 33.24 kcal/mol. Other paths lead to the formation of $CH_2 + I^-\cdots HCl$ (74.58 kcal/mol) and $CH_2 + I^- + HCl$ (92.35 kcal/mol). CH_3 and ICl^- products are both in doublet states and together they can form a singlet or a triplet system, depending on their spin orientations; thus, these products can be obtained on a singlet PES. The $I^-\cdots HCl$ complex is in the singlet state; however, the ground state of CH_2 is triplet (by excitation, we can get singlet CH_2) leading to a triplet ground-state product channel. Our PES is a singlet PES; therefore, only singlet CH_2 formation is possible during the present simulations. These electronic structure issues may partially explain the relatively high (2.82 and 4.76 kcal/mol) deviances from the benchmark energies for the $CH_2 + I^-\cdots HCl$ and the $CH_3 + ICl^-$ products. For the iodine substitution, the relative energies obtained on the PES are in excellent agreement with the benchmark results, the difference is 0.41 kcal/mol at the products, while for the transition states and minima, the average absolute difference is only 0.16 kcal/mol. The front-side attack and double-inversion transition states only differ with 0.19 and 0.73 kcal/mol from the benchmark energies, respectively. In the higher energy region, the proton-abstraction transition states and minima have an average error of 0.83 kcal/mol, while the products have a 0.54 kcal/mol difference. Even in the 80–100 kcal/mol region, we have a good accuracy of 1.08 kcal/mol for the HSubTS and 0.73 kcal/mol for the hydride-substitutionhydride-substitution products.

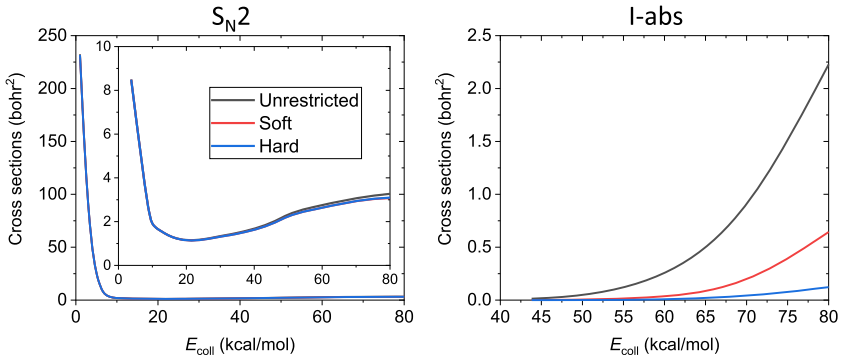

FIG. 3. Integral cross sections of the $Cl^- + CH_3I$ reaction for the S_N2 and iodine-abstraction channels without and with zero-point energy restrictions as a function of collision energy. The details of the restrictions can be found in Sec. II.

B. Integral cross sections and reaction probabilities

The integral cross sections of the $Cl^- + CH_3I$ reaction for S_N2 and iodine-abstraction channels can be seen in Fig. 3. Until about 20 kcal/mol collision energy, we can observe a decrease in the ICS. This can be explained by the fact that this reaction path is barrierless (as can be noticed in Fig. 2), and the attractive ion–dipole interactions make the reaction happen also at large impact parameters. However, if we increase the collision energy, we reduce the available time for these interactions to proceed with the reaction (forming the reactive orientation); thus, the ICS decreases. However, over 20 kcal/mol collision energy, we observe a slight increase in the ICS, which could be explained by the opening of another reaction pathway leading to the same products, but only a few S_N2 trajectories showed a retention mechanism, so that is not the case. Almost every trajectory fulfills the ZPE restrictions as expected since the reaction is exothermic and we gain vibrationally excited products. The few ZPE violating trajectories occur at higher collision energies as the reaction becomes more direct, leading to less internal excitation in the products. As for the iodine abstraction, the ICS starts to increase as we have more collision energy than the reaction heat (33.24 kcal/mol on this PES) of this reaction. The lowest E_{coll} where we see a small iodine-abstraction reactivity is 43.81 kcal/mol and there is a large increase as we move forward to higher collision energies as expected due to the endothermic nature. Most of the trajectories violate the ZPE restrictions, suggesting that we have less product internal excitation than in the case of the S_N2 reaction. We should note that our PES is not as accurate for the iodine-abstraction reaction channel as for the S_N2; thus, our results might have higher uncertainty for the former.

Regarding the reaction probabilities (Fig. 4), we can find analogous conclusions to the ones found in the case of the ICSs. For the S_N2 reactions, we have the largest reaction probability and maximum impact parameter (b_{max}) at the lowest collision energy (1 kcal/mol). The reason behind that is again the ion–dipole interaction because if the reactants reach each other with small velocity, there is time for proper attraction and alignment even from large distances. The reaction probability remains the same until we increase the impact parameter to about 12 bohrs (rebound mechanism), from that b, we have a monotonous decrease, and from 17 bohrs, a plateau until 22 bohrs (stripping mechanism), then again a monotonous decrease. With higher E_{coll}, the reaction probabilities drop as well as b_{max}, as the attraction does not have enough time to make the reaction happen. However, a slight increase can be seen in the probabilities if we move on to higher collision energies than 20 kcal/mol in agreement with the shape of the ICS curve. For the iodine-abstraction pathway, the reaction probability increases along with the collision energy because of the endothermic nature, while b_{max} is practically independent of E_{coll}.

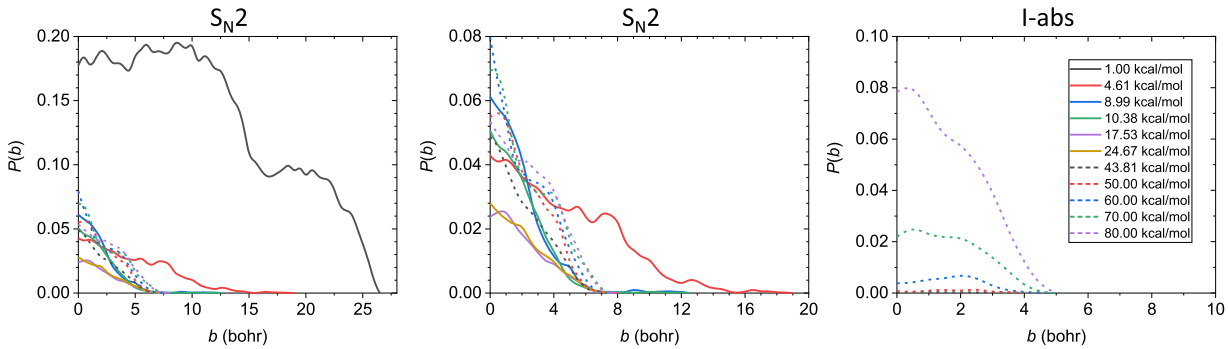

FIG. 4. Reaction probabilities of the $Cl^- + CH_3I$ reaction for the S_N2 and iodine-abstraction channels as a function of impact parameter at different collision energies. Solid line means that only the S_N2 products are formed, while the dashed line represents the appearance of the iodine-abstraction products.

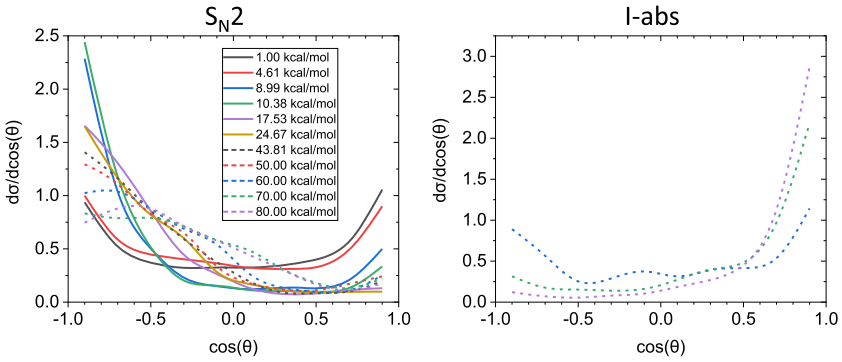

FIG. 5. Normalized scattering angle distributions of the $Cl^- + CH_3I$ reaction for the S_N2 and iodine-abstraction channels at different collision energies. Solid line means that only the S_N2 products are formed, while the dashed line represents the appearance of the iodine-abstraction products. Due to the low reaction probabilities (thus large statistical errors), we do not include the data obtained at 43.81 and 50.00 kcal/mol collision energies for iodine abstraction.

Based on visual inspection of selected S_N2 trajectory animations, we find that the reaction at low E_{coll} rarely proceeds via the roundabout mechanism[2] as the CH_3I has plenty of time to be aligned, whereas this mechanism becomes more and more significant as E_{coll} increases, especially at small b values (≲4.5 bohrs), where about 15–30% of the S_N2 reactions happen through the roundabout mechanism at E_{coll} of 17.5–50.0 kcal/mol. At E_{coll} = 70 kcal/mol, close to half of the S_N2 trajectories proceed with roundabout if $b \leq 4.5$ bohrs. Nevertheless, a detailed, E_{coll}- and b-dependent mechanism analysis of thousands of reactive S_N2 trajectories would require the development of a numerical protocol to identify the roundabout pathways, which is out of the scope of the present study.

C. Scattering and initial attack angle distributions

The normalized scattering angle distributions [cos(Θ)] can be seen in Fig. 5. For the S_N2 pathway, the angular distributions are backward–forward symmetric at low collision energies, while the backward scattering becomes more prevailing with increasing E_{coll}, but not completely monotonous. The dominance of the

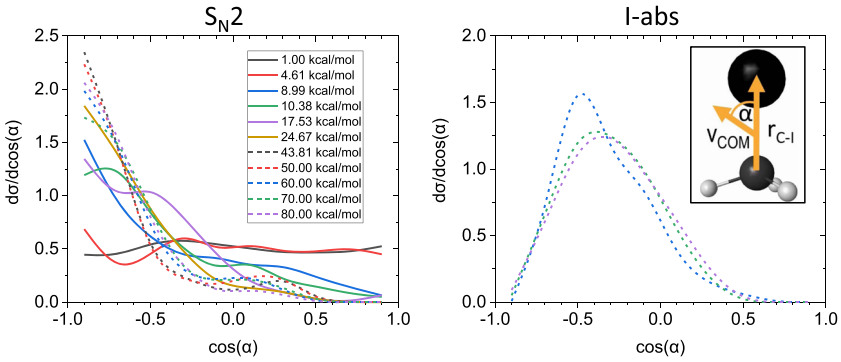

FIG. 6. Normalized initial attack angle distributions (definition can be seen in the inset graph or in Fig. 1) of the $Cl^- + CH_3I$ reaction for the S_N2 and iodine-abstraction channels at different collision energies. Solid line means that only the S_N2 products are formed, while the dashed line represents the appearance of the iodine-abstraction products. Due to the low reaction probabilities (thus large statistical errors), we do not include the data obtained at 43.81 and 50.00 kcal/mol collision energies for iodine abstraction.

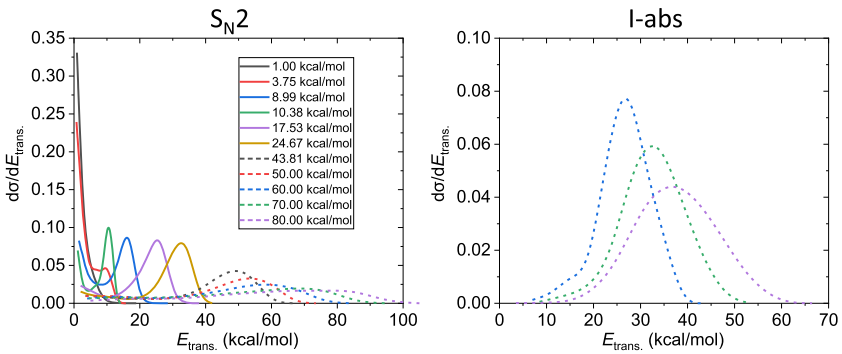

FIG. 7. Normalized product relative translational energy distributions of the $Cl^- + CH_3I$ reaction for the S_N2 and iodine-abstraction channels at different collision energies. Solid line means that only the S_N2 products are formed, while the dashed line represents the appearance of the iodine-abstraction products. Due to the low reaction probabilities (thus large statistical errors), we do not include the data obtained at 43.81 and 50.00 kcal/mol collision energies for iodine abstraction.

backward scattering is a feature of the direct rebound mechanism. Large impact parameters suggest forward scattering, while small b means backward scattering. At the smallest collision energies, we have a large maximal impact parameter; thus, the forward scattering is also significant, but as we increase the energy, the b_{max} becomes smaller and the forward scattering becomes less and less favored. Regarding the iodine abstraction, we do not plot the curves belonging to the 43.81 and 50.00 kcal/mol collision energies because the low reaction probability leads to large statistical error. With increasing E_{coll}, we see increased forward scattering, which suggests stripping mechanism.

In Fig. 6, the normalized initial attack angle distributions [cos(α)] can be seen. At small collision energies for the S_N2 reaction, the curves are isotropic, indicating that the reaction is indirect. Due to the small center of mass velocities, the initial attack angle is not important for the success of the reaction as there is plenty of time for the ion–dipole interactions to align the reactants into reactive orientation. As E_{coll} increases (the velocities as well), this time decreases; thus, the back-side attack will be dominant. In the case of the iodine abstraction, there is a side-on attack preference, in accordance with forward scattering (direct stripping mechanism). It is worth emphasizing that front-side (I-side) attacks do not lead to iodine abstraction, which is an interesting finding of the present simulations.

D. Product relative translational energy and internal energy distributions

The product relative translational energy distributions can be seen in Fig. 7. The curves belonging to the S_N2 reaction show a broadening tendency with increasing collision energies and the location of the maxima shifts roughly by the difference in the E_{coll}, showing that the translational energy transfer is significant. For the iodine abstraction, the curves are much colder; however, the translational energy transfer is also significant. As expected, most of the collisional energy is consumed by the endothermic reaction heat.

Normalized product internal energy ($E_{int.}$) distributions of the S_N2 reaction can be found in Fig. 8. At low collision energies, the location of the maxima is near the maximal internal energy

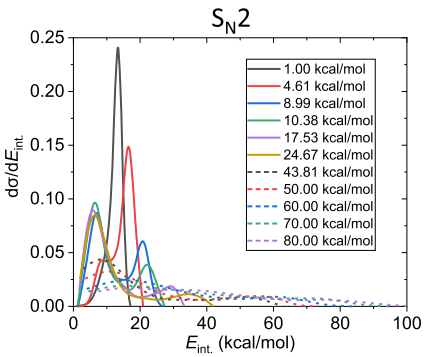

FIG. 8. Normalized product internal energy distributions of the $Cl^- + CH_3I$ reaction for the S_N2 channel at different collision energies. Solid line means that only the S_N2 products are formed, while the dashed line represents the appearance of the iodine-abstraction products. $E_{int.}$ is relative to the ZPE of the CH_3Cl product (23.87 kcal/mol on our PES).

suggesting an indirect reaction. With increasing E_{coll}, the location of the maximum shifts toward lower $E_{int.}$, indicating that the reaction becomes more direct. The small number of ZPE violations for the S_N2 reaction is in agreement with the fact that the $E_{int.}$ distributions, where $E_{int.}$ is relative to the ZPE of the CH_3Cl product (23.87 kcal/mol on our PES), show virtually zero populations if $E_{int.} < 0$.

E. Comparison with experimental and other theoretical data

The most comprehensive joint experimental–theoretical study on the title reaction was reported in 2013.[4] The Wester group performed state-of-the-art crossed-beam measurements, whereas theoretical simulations were done by the Hase group with MP2 and DFT/BHandH direct dynamics simulations at different vibrational and rotational temperatures. The reaction probabilities predicted by the MP2-based direct dynamics simulations are burdened with high uncertainty, and agree neither in the probability nor in b_{max} values derived from our simulations, especially at the lowest collision energies. The fact that MP2 underestimates the CCSD(T) S_N2 reactivity, which is here seen at the lowest E_{coll}, was also found in the case of the $F^- + CH_3I$ reaction.[28] The DFT simulations show similar or larger probabilities as our results; however, the maximal b is still not in agreement. The direct dynamics results for the scattering angle distribution were reported at 0.20 and 0.39 eV collision energies.[4] The high statistical uncertainty of the direct dynamics results hinders quantitative comparison with the present statistically well-converged differential cross sections. Nevertheless, both the previous[4] and present theoretical results show backward scattering preference at E_{coll} = 0.39 eV and isotropic scattering at E_{coll} = 0.2 kcal/mol.

Table I contains the comparison of the internal energy fractions between previous experimental and theoretical results[4] and our findings. Experiment and both simulations show, in qualitative or semi-quantitative agreement, that at low collision energies, the available energy mainly transfers into the product's internal motions, whereas at higher E_{coll} the internal excitation is less than the relative translational energy. The largest deviation between theory and experiment is seen at E_{coll} = 0.39 eV, where the measured internal energy fraction is 84%, whereas the previous/present simulations give 51/55%. Hase and co-workers[4] concluded that the experiment may have overestimated the collision energy of 0.39 eV because theory gave 86% at 0.2 eV, close to the value of 84% measured at 0.39 eV. Our result (79% at 0.2 eV) also confirms this belief.

TABLE I. Comparison of the experimental and theoretical internal energy fractions (in %, relative to the total available energy) at different collision energies.

E_{coll} (eV)	Experiment[a]	Previous simulations[b]	Present work
1.9	40	38 ± 5	31
1.07	25	···	30
0.76	40	46 ± 8	35
0.39	84	51 ± 4	55
0.2	···	86 ± 3	79

[a]Crossed-beam experimental results taken from Ref. 4.
[b]Direct dynamics results taken from Ref. 4.

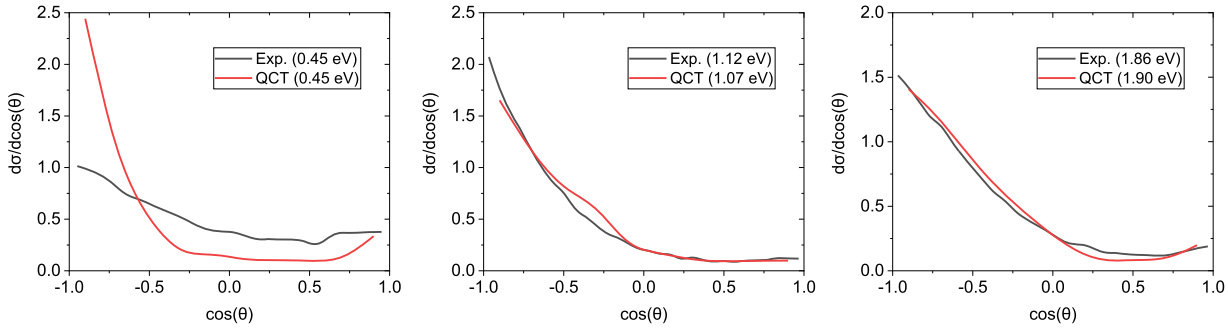

FIG. 9. Comparison of experimental[2,4,7] and computed normalized scattering angle distributions of the $Cl^- + CH_3I$ S_N2 reaction at three different collision energies.

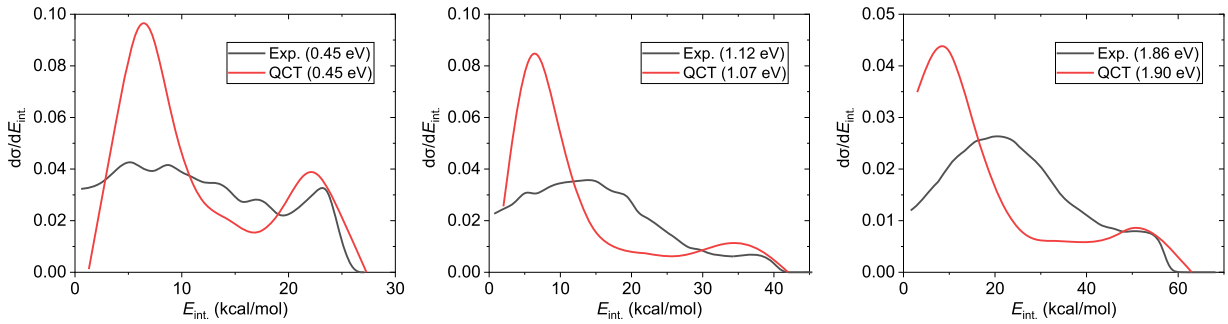

FIG. 10. Comparison of experimental[2,4,7] and computed normalized product internal energy distributions of the $Cl^- + CH_3I$ S_N2 reaction at three different collision energies.

We can directly compare the experimental[2,4,7] and theoretical differential cross sections in the case of the scattering angle and the internal energy. In Fig. 9, the experimental and computed scattering angle distributions can be seen at three different collision energies. At the two higher energies (~1.1 and 1.9 eV), we have an excellent, almost quantitative agreement, while at the lowest one (~0.5 eV), we can observe more backward scattering in the QCT simulations. The experimental and computed product internal energy distributions can be seen in Fig. 10. The simulations qualitatively reproduce the experimental features, but the QCT distributions are much colder, suggesting a more direct reaction than the experiments.

IV. SUMMARY AND CONCLUSIONS

Following our previous work on halide + methyl-halide reactions,[29–31] we have successfully developed a reactive PES for the $Cl^- + CH_3I$ system. The PES has been automatically constructed using the ROBOSURFER program system,[17] and the energy points have been fitted with the permutationally invariant-polynomial method[18,19] utilizing a high-level, composite, explicitly correlated coupled-cluster method with Brueckner (T) contributions, using the aug-cc-pVTZ(-PP) basis set. Our singlet state PES describes different kinds of reactions, whereas QCT computations have shown that two of them are significant in the investigated collision energy range (1–80 kcal/mol): the S_N2 and the iodine abstraction. The integral cross sections show that the substitution reaction is present at all of the investigated E_{coll}-s, whereas the abstraction channel opens at around 45 kcal/mol. Normalized scattering angle and initial attack angle distributions show that for the S_N2 reaction initially there is both backward and forward scattering, but with increasing collision energies, the backward scattering becomes more dominant whereas for the abstraction, we can see a clear preference for forward scattering. The initial attack angle distributions show that the formation of iodine–ion happens without initial orientation preference at low E_{coll}, whereas the back-side (CH_3-side) attack becomes more and more dominant as E_{coll} increases, whereas the abstraction has a side-on/back-side attack preference. The product relative translational energies show that the translational energy transfer is significant in both cases. For the S_N2 channel, the product internal energy distributions show negligible ZPE violation and the shapes of the distributions indicate a shift from indirect to direct dynamics with increasing E_{coll}. The present statistically converged differential cross sections have allowed direct comparison with crossed-beam experiments.[2,4,7] For some cases (scattering angle distributions at high E_{coll}) excellent quantitative agreement has been found, whereas in other cases (scattering angle distributions at low E_{coll} and product internal energy distributions) theory has only qualitatively reproduced experiment. The present simulations are more robust than previous direct dynamics computations;[4] nevertheless, both theoretical approaches provide qualitatively similar conclusions. The remaining differences between theory and experiment may motivate further computations and measurements.

SUPPLEMENTARY MATERIAL

See the supplementary material for codes for PES evaluation (Ref. 18).

ACKNOWLEDGMENTS

We thank the National Research, Development and Innovation Office (NKFIH, Grant No. K-125317); Project No. TKP2021-NVA-19 provided by the Ministry of Innovation and Technology of Hungary from the National Research, Development and Innovation Fund, financed under the TKP2021-NVA funding scheme; and the Momentum (Lendület) Program of the Hungarian Academy of Sciences for financial support. The authors thank Dr. Bastiaan Braams for giving them permission to share the PES libraries as the supplementary material and Dr. Tim Michaelsen and Professor Roland Wester for sending them the experimental data.

AUTHOR DECLARATIONS

Conflict of Interest

The authors have no conflicts to disclose.

Author Contributions

András B. Nacsa: Data curation (lead); Formal analysis (lead); Investigation (lead); Methodology (lead); Software (lead); Validation (lead); Visualization (lead); Writing – original draft (lead); Writing – review & editing (equal). **Viktor Tajti**: Formal analysis (supporting); Investigation (supporting); Methodology (supporting); Software (supporting); Validation (supporting); Writing – review & editing (supporting). **Gábor Czakó**: Conceptualization (lead); Funding acquisition (lead); Methodology (supporting); Project administration (lead); Supervision (lead); Validation (supporting); Writing – original draft (supporting); Writing – review & editing (equal).

DATA AVAILABILITY

The data that support the findings of this study are available from the corresponding author upon reasonable request.

REFERENCES

[1]W.-P. Hu and D. G. Truhlar, J. Am. Chem. Soc. **117**, 10726 (1995).
[2]J. Mikosch, S. Trippel, C. Eichhorn, R. Otto, U. Lourderaj, J. X. Zhang, W. L. Hase, M. Weidemüller, and R. Wester, Science **319**, 183 (2008).
[3]J. Zhang, U. Lourderaj, S. V. Addepalli, W. A. de Jong, and W. L. Hase, J. Phys. Chem. A **113**, 1976 (2009).
[4]J. Zhang, U. Lourderaj, R. Sun, J. Mikosch, R. Wester, and W. L. Hase, J. Chem. Phys. **138**, 114309 (2013).
[5]I. Szabó and G. Czakó, J. Phys. Chem. A **121**, 5748 (2017).
[6]P. Liu, C. Li, and D. Wang, J. Phys. Chem. A **121**, 8012 (2017).
[7]E. Carrascosa, J. Meyer, T. Michaelsen, M. Stei, and R. Wester, Chem. Sci. **9**, 693 (2018).
[8]S. Pratihar, M. C. Nicola Barbosa Muniz, X. Ma, I. Borges, Jr., and W. L. Hase, Phys. Chem. Chem. Phys. **21**, 2039 (2019).
[9]X. Ji, C. Zhao, and J. Xie, Phys. Chem. Chem. Phys. **23**, 6349 (2021).
[10]J. Zhang, J. Mikosch, S. Trippel, R. Otto, M. Weidemüller, R. Wester, and W. L. Hase, J. Phys. Chem. Lett. **1**, 2747 (2010).
[11]J. Xie, J. Zhang, and W. L. Hase, Int. J. Mass Spectrom. **378**, 14 (2015).
[12]M. Stei, E. Carrascosa, M. A. Kainz, A. H. Kelkar, J. Meyer, I. Szabó, G. Czakó, and R. Wester, Nat. Chem. **8**, 151 (2016).
[13]J. Xie and W. L. Hase, Science **352**, 32 (2016).
[14]I. Szabó and G. Czakó, Nat. Commun. **6**, 5972 (2015).
[15]I. Szabó and G. Czakó, J. Phys. Chem. A **119**, 3134 (2015).
[16]I. Szabó, B. Olasz, and G. Czakó, J. Phys. Chem. Lett. **8**, 2917 (2017).
[17]T. Győri and G. Czakó, J. Chem. Theory Comput. **16**, 51 (2020).
[18]B. J. Braams and J. M. Bowman, Int. Rev. Phys. Chem. **28**, 577 (2009).
[19]J. M. Bowman, G. Czakó, and B. Fu, Phys. Chem. Chem. Phys. **13**, 8094 (2011).
[20]T. H. Dunning, Jr., J. Chem. Phys. **90**, 1007 (1989).
[21]K. A. Peterson, D. Figgen, E. Goll, H. Stoll, and M. Dolg, J. Chem. Phys. **119**, 11113 (2003).
[22]T. B. Adler, G. Knizia, and H.-J. Werner, J. Chem. Phys. **127**, 221106 (2007).
[23]K. A. Brueckner, Phys. Rev. **96**, 508 (1954).
[24]D. A. Tasi, T. Győri, and G. Czakó, Phys. Chem. Chem. Phys. **22**, 3775 (2020).
[25]H.-J. Werner, P. J. Knowles, G. Knizia, F. R. Manby, M. Schütz *et al.*, MOLPRO, version 2015.1, a package of *ab initio* programs, see http://www.molpro.net.
[26]W. L. Hase, *Encyclopedia of Computational Chemistry* (Wiley, New York, 1998), pp. 399–407.
[27]P. Papp, V. Tajti, and G. Czakó, Chem. Phys. Lett. **755**, 137780 (2020).
[28]T. Győri, B. Olasz, G. Paragi, and G. Czakó, J. Phys. Chem. A **122**, 3353 (2018).
[29]I. Szabó and G. Czakó, J. Phys. Chem. A **121**, 9005 (2017).
[30]G. Czakó, T. Győri, B. Olasz, D. Papp, I. Szabó, V. Tajti, and D. A. Tasi, Phys. Chem. Chem. Phys. **22**, 4298 (2020).
[31]V. Tajti, T. Győri, and G. Czakó, J. Chem. Phys. **155**, 124301 (2021).